SLAC-PUB-11493
September 2005

EXPERIMENTAL STUDIES OF TEMPORAL ELECTRON BEAM SHAPING AT THE DUV-FEL ACCELERATOR

H. Loos*, D. Dowell, SLAC, Menlo Park, CA 94025, USA
B. Sheehy†, Y. Shen, T. Tsang, X. Wang, BNL, Upton, NY 11973, USA
L. Serafini, INFN-Milano, Milan, Italy
M. Boscolo, M. Ferrario, M. Petrarca, C. Vicario, INFN/LNF, Frascati (Rome), Italy

Abstract

The photoinjectors for future short wavelength high brightness accelerator driven light sources need to produce an electron beam with ultra-low emittance. At the DUV-FEL facility at BNL, we studied the effect of longitudinally shaping the photocathode laser pulses on the electron beam dynamics. We report on measurements of the longitudinal phase space distributions and the time-resolved transverse beam parameters for both a Gaussian and a flat-top temporal laser pulse profile.

INTRODUCTION

The brightness and performance of future X-ray FEL light sources is limited by the brightness of the driving electron beam. The requirements on transverse and longitudinal emittance are expected to be met with the electron beam generated by a photoinjector. The typical Gaussian temporal shape of the photocathode drive laser results in growth of both longitudinal and transverse emittance due to space charge forces. One way of mitigating these effects is to use a flat-top temporal distribution for the drive laser to eliminate the longitudinal space charge force within the bunch and to have a uniform transverse space charge force [1].

In this paper we report on an experiment conducted at the DUV-FEL facility at BNL in collaboration with the SPARC project at INFN-LNF and LCLS at SLAC, where an acousto-optical programmable dispersive filter (DAZZLER from FASTLITE) [2] was used to shape the time distribution of the photocathode drive laser [7]. A non-shaped Gaussian, and a shaped flat-top laser distribution were generated to compare the electron beam properties at two different charges and two different shapes. The experimental results include the longitudinal phase space and the time resolved transverse emittance for these cases.

EXPERIMENTAL SETUP

The DUV-FEL accelerator [3] consists of a BNL/SLAC/UCLA 1.6 cell gun and 5 SLAC-type 2856 MHz accelerating structures providing up to 250 MeV beam energy [4]. The gun is driven by a frequency-tripled Ti:Sapphire amplifier operating at 10 Hz. A 4 dipole chicane after the second linac tank enables bunch compression at 70 MeV. Downstream of the accelerating structures is a dipole spectrometer magnet followed in the straight direction by the two undulators for the HGHG experiment [5]. When the dipole is powered, the energy distribution of the electron beam can be monitored on a Ce:YAG view-screen with a CCD camera. View-screens and quadrupoles along the linac enable the measurement of the projected transverse emittance. Time-resolved measurements are possible by measuring the energy spectrum of the electron beam at off-crest or zero-crossing phase in the last used accelerating structure [6]. By varying the phase or amplitude of this structure, the longitudinal phase space distribution can be determined. The time resolved transverse beam parameters or slice emittances are obtained by changing an upstream quadrupole and measuring the vertical beam sizes after the horizontally dispersing spectrometer dipole. The energy coordinate of the dispersed beam can be mapped onto the time coordinate with the energy-time correlation of the longitudinal phase space distribution.

The Ti:Sapphire laser system and the implementation of the pulse shaping with the DAZZLER device has been de-

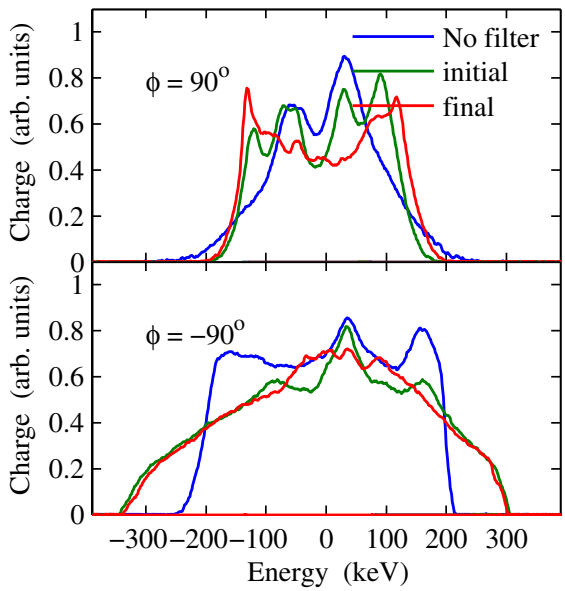

Figure 1: Energy spectra of the 70 pC electron bunch without shaping, with the initial and the optimized laser pulse for positive and negative chirp.

* loos@slac.stanford.edu
† on leave

Contributed to 27th International Free Electron Laser Conference (FEL 2005) , 21-26 Aug 2005, Stanford, California

Work supported in part by Department of Energy contract DE-AC02-76SF00515

scribed in [7]. The parameters of the laser beam were 4.8 ps FWHM for the gaussian pulse and 7.8 ps for the flat-top pulse. Two cases for the electron beam were studied, one with a charge of 70 pC (low charge) and one with a charge of 300 pC (high charge). The electron beam was accelerated with the first two linac structures to an energy of 65 MeV. The rf-phases of these structures were set to obtain maximum energy and minimum energy spread in the spectrometer with the remaining structures turned off. The chicane was not powered during this experiment. Either the third or the fourth accelerating structure was used to add a calibrated energy chirp to the beam at both of the rf zero-crossings, i.e., at $\pm 90^\circ$ of the phase for the time-resolved measurements.

The lack of a single shot high resolution temporal diagnostic for the UV laser pulses made it necessary to use the electron beam energy spectrum as diagnostic to improve the flatness of the shaped laser pulse. The energy spectra of the electron beam with no shaping, with the initial laser shape and the optimized laser shape are shown in Fig. 1 for both rf zero-crossings. The Gaussian pulse without shaping has a temporal modulation (see Fig. 2) which is also visible in the spectrum at $+90^\circ$ phase. The initial shaping was done by applying a 8 nm wide square amplitude filter to the DAZZLER resulting in a laser pulse with short 1 ps long edges, but the modulation from the Gaussian pulse still present. By changing the shape of the amplitude filter while observing the electron beam spectrum, the modulation in the spectrum could be removed. The amplitude was sampled with 12 bins over 8 nm, representing the 0.6 nm resolution of the DAZZLER. The required changes to the amplitude bins where not larger than 5%, which shows the sensitivity of the Ti:Sapphire amplifier and the UV conversion to spectral and temporal structure in the seed pulse.

LONGITUDINAL PHASE SPACE

The longitudinal phase space distribution can be reconstructed with tomographic methods from a suitable set of energy spectra obtained for different chirps [8]. The slice energy spread, the energy-time correlation, and the current distribution can then be calculated from the phase space distribution. Using a method related to the one described in [9], the energy-time correlation and the charge distribution can be determined from two energy spectra measured at large chirps with opposing signs. The method is based on the assumptions that the chirps are large enough to provide a monotonic energy time relation for both projections and that the slice energy spread is small compared to the energy spread of the chirped projections. Both assumptions are usually met at the DUV-FEL accelerator.

The energy-time correlation of the beam with applied chirps $k_{1,2}$ at the two rf zero-crossing phases is

$$E_{1,2}(t) = \Delta E(t) + k_{1,2} t \tag{1}$$

for an initial energy-time correlation of $\Delta E(t)$ and k_1 being positive and k_2 negative. The measured energy spectra are $\rho_{1,2}(E)$. The charge as a function of energy

$$Q(E_{1,2}) = \int_{-\infty}^{\pm E_{1,2}} \rho_{1,2}(\pm E)\, dE \tag{2}$$

is obtained by integrating both spectra starting at the bunch head. This requires reverting the energy axis for the negative chirp k_2. By using the charge Q as a variable, the energy $E_{1,2}(Q)$ for a given charge, i.e., location in the bunch, can be identified in both spectra. Using Eq. 1, the temporal location

$$t(Q) = \frac{E_1(Q) - E_2(Q)}{k_1 - k_2} \tag{3}$$

is determined as a function of charge. The current distribution is then

$$I(t) = \frac{dQ(t)}{dt} = \rho_1(E_1(t)) \frac{dE_1(t)}{dt} \tag{4}$$

and the initial energy-time correlation is

$$\Delta E(t) = \frac{E_2(Q(t))\, k_1 - E_1(Q(t))\, k_2}{k_1 - k_2}\,. \tag{5}$$

The effect of phase jitter and drift is less severe in this method compared to tomography where errors in the chirp lead to artifacts in the reconstruction. Using only two energy spectra, errors in the chirps $k_{1,2}$ result in an error of the scaling of the time coordinate and in a linear chirp contribution to the initial energy-time correlation ΔE. It has no

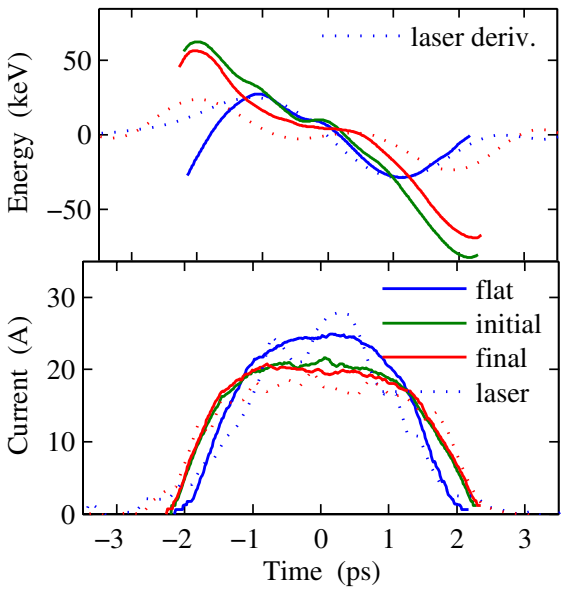

Figure 2: Energy-time correlation and current distribution obtained from the energy spectra shown in Fig. 1. The laser distributions are scaled by 0.5 in time. The dotted lines in the top figure are smoothed derivatives of the laser shapes scaled to match the respective energy correlations.

influence on the bunch structure or the higher order energy-time correlations.

Applying this method to the energy spectra from Fig. 1 gives the energy correlation and current distribution shown in Fig. 2. The time scale for the laser pulse was divided by two to account for rf-compression of the electron beam. The different shapes of the Gaussian and the flat-top laser pulses and the structure within the laser pulses are not visible in the current distributions which are close to parabolic distributions due to the space charge forces. The change from the initial to the optimized flat-top pulse has almost no influence on the current distribution. The laser pulse shape however is closely related to the energy-time correlation. The modulation in the laser pulse is visible as a modulation in the energy-time correlation. The different signs of the curvature in the tails of the laser pulse distributions correspond to the different slopes of the energy-time correlation of the Gaussian and flat-top pulse. This relation can be explained as the effect of the longitudinal space charge force which is proportional to the derivative of the current distribution [10]. The dotted lines in the energy-time correlation are appropriately scaled and smoothed derivatives of the laser pulse distributions which qualitatively describe the observed energy-time correlations.

Tomographic reconstructions were made from sets of energy spectra obtained by changing the accelerating gradient for both $+90^o$ and -90^o phase in linac tank 3 for the 70 pC and in tank 4 for the 300 pC case. Both the Gaussian laser pulse without shaping and the optimized flat-top pulse were studied. The results from the tomographic reconstruction for 70 pC are shown in Figs. 3 and the corresponding energy-time correlations and current distributions in Fig. 4. The phase space shows a linear correlation for most of the charge in the flat-top case, whereas the Gaussian pulse shows higher order correlation within the entire bunch. The energy-time correlation is similar to the results obtained with the method described earlier. The main difference is the linear correlation term because the reconstructed phase space is shown with a chirp such that the energy spread is at minimum. The current distribution from the phase space reconstruction exhibits more structure which are due to artifacts in the reconstruction from phase and amplitude drifts during the data acquisition.

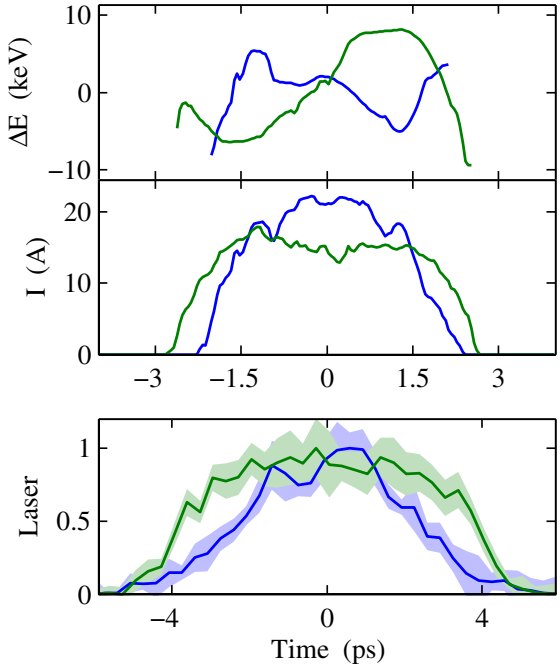

Figure 4: Time distributions from phase space reconstruction of the 70 pC beam. Blue indicates the Gaussian, green the flat-top case. The top panel shows the correlation between slice energy vs. time, the middle shows the current distribution, and the bottom the corresponding UV laser pulse distributions.

The tomographic reconstruction for the 300 pC case is shown in Fig. 5 with the energy-time correlation and current distribution in Fig. 6. The correlation for the Gaussian pulse with no shaping is the same as for the 70 pC case. The structure visible in the flat-top phase space is mostly a result of reconstruction artifacts due to poor stability of the drive laser during this part of the experiment. The current distributions of both pulse shapes differ less compared to the 70 pC case because of the higher charge.

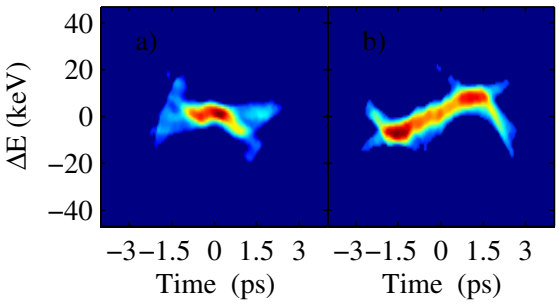

Figure 3: Longitudinal phase space reconstructions for 70 pC. Panel a) shows the Gaussian, b) the flat-top case.

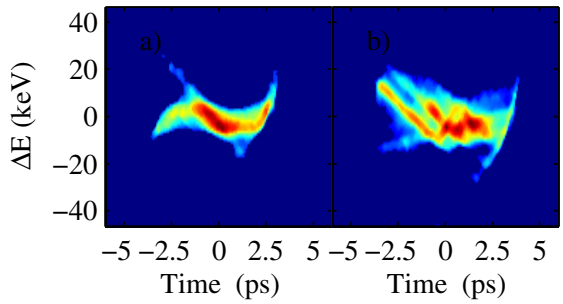

Figure 5: Longitudinal phase space reconstructions for 300 pC. Panel a) shows the Gaussian, b) the flat-top case.

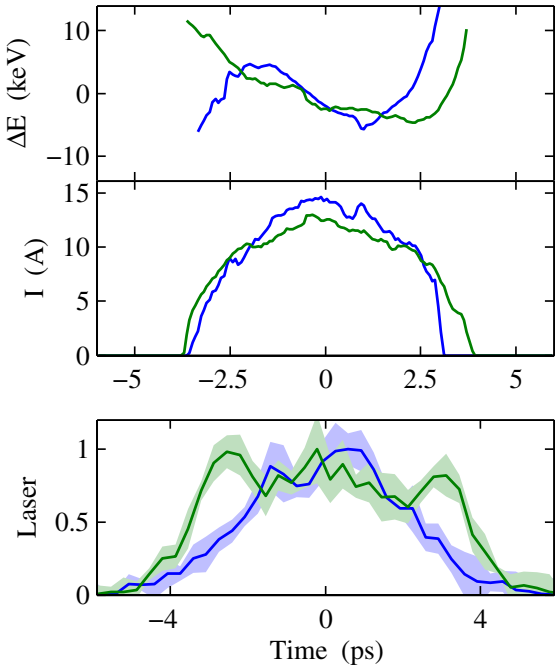

Figure 6: Time distributions from phase space reconstruction of the 300 pC beam similar to Fig. 4.

TRANSVERSE BEAM PARAMETERS

The results of the time resolved emittance measurements are shown in Fig. 7 for the 70 pC and in Fig. 8 for the 300 pC case. In each case the energy coordinate from the spectrum was converted into a time coordinate using the energy-time correlation from the longitudinal measurements and Eq. 5. The mismatch parameter $\xi = (\gamma_0\beta - 2\alpha_0\alpha + \beta_0\gamma)/2$ is a measure for the relative alignment of the transverse beam ellipses with the central slice taken as reference. In the low charge case, the slice emittance of 1.4 μm is the same for both pulse shapes, but the projected emittance of 1.7 μm is larger for the Gaussian pulse due to misalignment of the slices in the tails of the distribution.

In the high charge case for 300 pC, the projected emittance was measured with the three screen method and is 2.0 μm for the Gaussian shape and 1.5 μm for the flat-top pulse. The slice emittance measurement for the Gaussian pulse agrees with the measurement of the projected emittance. The slice emittance of the flat-top pulse however is systematically too high because the electron beam was focused too tightly in the spectrometer screen, thus exceeding the screen resolution. As in the low charge case, most of the slices for the 300 pC flat-top pulse are well aligned.

SUMMARY

The longitudinal and time-resolved transverse beam parameters of the electron beam generated by a Gaussian and a flat-top laser profile were measured in this study, showing an improvement of the projected transverse emittance and the longitudinal phase space linearity by the shaping due to the better uniformity of the laser pulse shape.

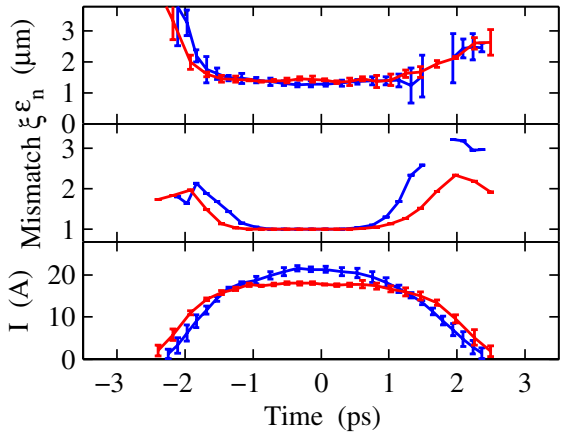

Figure 7: Vertical slice emittances for 70 pC in the top part. Blue indicates the Gaussian, red the flat-top case. The center part shows the mismatch parameter and the bottom contains the current distribution.

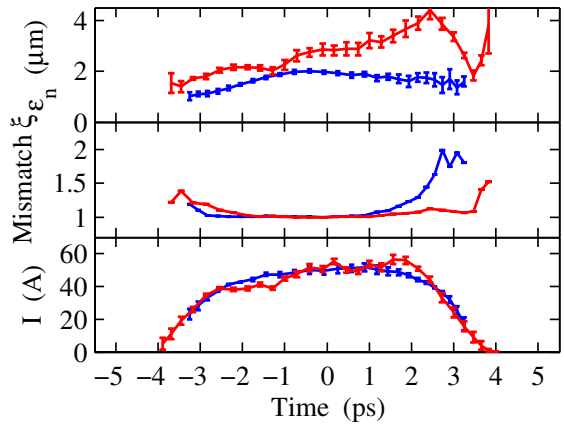

Figure 8: Vertical slice emittances for 300 pC similar to Fig. 7.

This work was supported by DOE Contracts DE-AC03-76SF00515 and DE-AC02-98CH10886.

REFERENCES

[1] J. Yang et al., EPAC 2002, Paris, June 2002, p. 1828

[2] F. Verluise et al., Opt. Lett. **25** (2000) 575

[3] W. S. Graves et al., PAC 2001, Chicago, June 2001, p. 2860

[4] X.J. Wang et al., PAC 2005, Knoxville, May 2005, TOAB003

[5] L.H. Yu et al., Phys. Rev. Lett. **91** (2003) 074801

[6] W. S. Graves et al., PAC 2001, Chicago, June 2001, p. 2224

[7] H. Loos et al., PAC 2005, Knoxville, May 2005, MOPB008

[8] H. Loos et al., Nucl. Instrum. Meth. A 528 (2004) 189

[9] K. L. F. Bane, SLAC/AP-80 (1990)

[10] A. W. Chao, "Physics of Collective Beam Instabilities in High Energy Accelerators", Wiley, New York (1993)